ANNALS OF GEOPHYSICS, 67, 6, S658, 2024; doi:10.4401/ag-9136
OPEN ACCESS

Application of the Stochastic Finite Fault Model in the Study of the Source Rupture Process of the Mw 7.6 Earthquake in the Noto Peninsula, Japan on January 1, 2024

Zhuofan Yang[*,1], Benyu Liu[1], Kui Liu[1]

(1) Yunnan University, School of Earth Sciences, Department of Geophysics, Yunnan Province, China

Article history: received August 6, 2024; accepted January 13, 2025

Abstract

On January 1, 2024, a Mw 7.6 earthquake occurred on the Noto Peninsula in Japan, with a focal depth of 9.6 kilometers. To validate the effectiveness of using a finite fault hybrid slip model to simulate strong ground motion events, this study utilized strong motion records from the KiK-net station network of the National Research Institute for Earth Science and Disaster Resilience (NIED) in Japan. Initially, 29 fundamental stations were selected, and 13 of these stations were chosen for further study using the finite fault method. Constrained by the geometric parameters of the initial model from the strong motion inversion, a hybrid slip distribution model (HSM) was established based on the stochastic finite fault model and semi-empirical relationships between source parameters. This model accurately reflects the spatial and temporal characteristics of the source rupture, and its results are comparable to those obtained by the United States Geological Survey (USGS) using GNSS and other long-period effect data. Additionally, using the dynamic corner frequency-based stochastic ground motion synthesis method (EXSIM), a comparative study was conducted on the pseudo-acceleration response spectra (PSA) of the hybrid slip model, the strong motion inversion model, and the source rupture model provided by USGS at the selected stations. These were then compared with the response spectra of actual station records. It was found that all three models showed good fitting results, and in the short-period range, the simulated values of the HSM were closer to the actual records. Finally, the relative error mean and variance between the HSM and actual records' PSA at different frequencies were calculated for 29 stations. It reveals that they still had good fitting results. Overall, the findings demonstrate that even without relying on extensive station data, the hybrid slip model efficiently and accurately simulated high-frequency strong ground motions near the fault with a damping ratio of 5%, verifying the reliability and applicability of this method.

Keywords: Hybrid sliding model; Ground motion simulation; Strong ground motion inversion; Source rupture process; Noto Peninsula

1. Introduction

The study of strong ground motion is fundamental to gain insight into the occurrence and development characteristics of surface vibrations during earthquakes and it is the key to reduce the impact of earthquake disasters. Particularly, determination of the source rupture process and establishment of the source model is crucial for strong ground motion studies. Its findings can be directly used for calibrating fundamental strong ground motion parameters and predicting ground motions.

The finite fault model is an effective method for studying the impact of the source rupture process on near-source or near-fault ground motions. For small and far-field ground motion simulations, where the size of the seismic source relative to the distance from the observation points is small, the point source model proposed by Boore (1983) is generally used. The spatial distribution of near-field ground motion is strongly influenced by the direction of the fault, the heterogeneous slip distribution on the rupture plane, and the dynamics of the rupture process. Therefore, it is necessary to establish a finite fault model to account for the impact of the source rupture process on near-source or near-fault ground motion. The existing finite fault kinematic models can be divided into deterministic source models (Olson and Aspel, 1982), stochastic source models (Andrews, 1981; Zeng et al., 1994) and hybrid source models (Wang, 2004; Jiang and Li, 2023). Deterministic source models are primarily used to define regions of high slip on fault planes; stochastic source models can describe complex phenomena of slip distribution with unknown patterns; hybrid slip models combine the advantages of deterministic and stochastic sources, utilizing deterministic source models to provide physical constraints for the parameters of stochastic source models and employing stochastic source models to generate high-frequency seismic source models that deterministic source models cannot express. Wang Haiyun (2004) developed a hybrid slip model that combines deterministic asperity modeling with a two-dimensional slip spectrum model (k^2 model) with random phase, to establish the slip of low and high wavenumbers on the fault. In the hybrid model, the two slip distributions are superimposed in the wavenumber domain, resulting in a composite slip model over the entire rupture surface. Based on this, to describe the influence of fault types on strong ground motion, Wang Haiyun (2004) further differentiated the scaling laws of global and local parameters for earthquakes on all faults, dip-slip faults, and strike-slip faults.

In the development of Wang Haiyun's (2004) hybrid slip model, the calibration of various source parameters is based on mathematical statistical principles, resulting in a certain degree of randomness. To reduce the impact of mathematical random differences on the simulation of the source rupture process, it is necessary to constrain the model with some real data to approximate the actual situation. Therefore, this study first uses the strong motion inversion method (Zheng et al., 2020; Zhang et al., 2013, 2017) and the strong motion data recorded by the KiK-net stations in Japan during the 2024 Noto Peninsula earthquake to obtain the initial model of the static source rupture process and the source time functions of the sub-faults. Based on the geometric parameters of the initial model and the rupture mode indicated by the time functions, combined with semi-empirical relations (Wang, 2004; Tao et al., 2009; Sun, 2010), global and local parameters are determined to establish the hybrid slip model.

Furthermore, using the aforementioned model and the stochastic finite fault method based on dynamic corner frequency (EXSIM), strong motion simulations were performed for selected stations in the study area. By comparing the pseudo-acceleration response spectra simulated by original records, inversion model, USGS model and HSM, the effectiveness of our method was validated. The results indicate that the method employed in this study also provides crucial input parameters for broadband seismic motion simulations and explores its potential applications in similar tectonic regions.

2. The Stochastic Finite Fault Method (SFF)

2.1 Fault Source Hybrid Slip Model

The establishment of the finite fault source model primarily involves determining the source parameters. According to Irikura (2000), the source model parameters are divided into global source parameters and local source parameters. The former represents the macroscopic characteristics of the source area, such as the spatial orientation of the seismic fault (position, dip, strike, depth), fault rupture scale (length, width, area), average slip on the fault plane, and average rupture velocity. The latter indicates the heterogeneity or roughness of the fault plane, primarily characterized by the slip distribution.

To more accurately describe this heterogeneity, the hybrid slip model has emerged. This model combines the characteristics of global and local source parameters. It reflects the complexity of fault rupture by appropriately distributing the slip across the fault surface. The following are the steps for establishing the hybrid slip model:

1) Based on geological background, seismic activity surveys, and geophysical exploration data, determine the spatial location and slip type of active faults. According to the specified moment magnitude (Mw), use seismic scaling laws to determine the global source parameters. Determine the asperity parameters through semi-empirical relationships.
2) Divide the fault rupture surface into 1.0 km × 1.0 km grids, determine the positions of the largest asperity and other asperities, and assign the corresponding slip values to each grid. Discretize the fault rupture surface into $2^M \times 2^N$ grids (2^M refers to the total number of grids along the strike direction of the fault, and 2^N refers to the total number of grids along the dip direction of the fault. The values of M and N are often chosen such that M = N), then perform interpolation and smoothing.
3) Use Fourier transform to convert the generated asperity model from the spatial domain to the wavenumber domain; when the wavenumber is greater than the spatial corner wavenumber, use a two-dimensional slip spectrum function with random phase (k^2 slip model) to generate a random slip distribution.

$$D(k_x, k_y) = \frac{\overline{D} \cdot L \cdot W}{\sqrt{1 + \left[\left(\frac{k_x L}{K}\right)^2 + \left(\frac{k_y W}{K}\right)^2\right]^2}} e^{i\Phi(k_x, k_y)} \tag{1}$$

Where k_x is the wavenumber along the strike direction of the rupture surface, k_y is the wavenumber along the dip direction, L and W are the length and width of the pseudo-fault rupture, $\overline{D}$ is the average slip amount, and $\Phi(k_x, k_y)$ is the random phase spectrum.

4) Combine the asperity model and the k^2 slip model in the wavenumber domain to generate a hybrid slip model. Finally, use the inverse Fourier transform to convert the hybrid slip model from the wavenumber domain back to the spatial domain, resulting in the spatial domain hybrid slip model.

2.2 The Stochastic Synthesis Method for Near-Fault Ground Motions

In the simulation of near-fault strong ground motions, the fault plane in the source model is divided into N equal-sized sub-faults. The rupture process propagates radially outward from the initiation point at a certain rupture velocity (generally 0.8 times the shear wave velocity). The ground motion caused by each sub-source is calculated using Boore's point-source model (1970, 2003). The ground motions from all sub-sources at the observation point are superimposed in the time domain with appropriate time delays to obtain the ground motion time history at the observation point.

$$a(t) = \sum_{i=1}^{N_L} \sum_{j=1}^{N_W} a_{ij}(t + \Delta t_{ij}) \tag{2}$$

Here, N_L and N_W are the number of sub-faults along the strike and dip directions, $N_L \times N_W = N$ is the total number of sub-sources; Δt_{ij} includes the time delay due to rupture propagation to the ij-th sub-source and the time delay due to different propagation distances from the ij-th sub-source to the site; $a_{ij}(t)$ is the ground motion at the observation point caused by the ij-th sub-source.

Motazedian (2005) proposed the stochastic finite fault method based on dynamic corner frequency, building on the stochastic point source method and the finite fault method with static corner frequency. This approach eliminates the influence of sub-fault size division on the simulation results of ground motion and resolves the issue of multiple ruptures within the same sub-fault during an earthquake. Consequently, the stochastic finite fault method has extended its applicability to a wider range of magnitudes.

This method describes the Fourier spectrum of acceleration at the target site, located at distance R_{ij} from the i-th row and j-th column sub-fault, in the frequency domain.

$$A_{ij}(f) = \left\{\frac{CM_{0ij}H_{ij}(2\pi f)^2}{1+\left(f/f_{0ij}\right)^2}\right\} \cdot \left\{\exp\left(-\frac{\pi f R_{ij}}{QB}\right) G\left(R_{ij}\right)\right\} \cdot \{\exp(-\pi\kappa f)A(f)\} \tag{3}$$

In the equation, the first term represents the source spectrum part. M_{0ij}, f_{0ij} and R_{ij} are respectively the seismic moment, corner frequency, and source distance of the i-th row and j-th column sub-fault to the target site, C is a frequency-independent proportion constant. The second term represents the path propagation part, including non-elastic attenuation $\exp\left(-\frac{\pi f R_{ij}}{QB}\right)$ and geometric spreading $G\left(R_{ij}\right)$, where Q is the quality factor of the propagation medium. The symbol β represents the shear wave velocity (km/sec) in the source region. The third term is the site response function, $\exp(-\pi\kappa f)$ indicating rapid decay of the high-frequency components of the source spectrum, and $A(f)$ represents amplification effects near the near-field. The symbol κ represents the high-frequency attenuation parameter. The spatial corner frequency of the sub-fault is represented as:

$$f_{0ij} = 4.9 \times 10^6 \beta \left(\frac{\Delta\sigma N}{N(t)M_0}\right)^{1/3} \tag{4}$$

In the equation, $\Delta\sigma$ represents the stress drop; M_0 is the seismic moment of the entire fault $N(t)$ is the sum of the number of sub-faults already ruptured at time t.

To ensure the conservation of high-frequency radiation energy, Motazedia (2005) introduced a high-frequency calibration factor H_{ij} to compensate for the underestimated far-field radiation energy of sub-faults. It can be represented as follows:

$$H_{ij}(f) = \sqrt{\frac{N\sum\{f^2/[1+(f/f_0)^2]\}^2}{\sum\left\{f^2/\left[1+\left(f/f_{w,ij}\right)^2\right]\right\}^2}} \tag{5}$$

3. Strong Motion Data Source and Inversion

3.1 Seismic Motion Record Filtering

The acceleration data used for simulating ground motion caused by the Mw7.6 earthquake in the Noto Peninsula were obtained from the KiK-net strong-motion seismograph network operated by the National Research Institute for Earth Science and Disaster Resilience (NIED) in Japan. Using the Automatic Inversion Codes program developed by Zhang Y. et al. (Zheng et al., 2020; Zhang et al., 2013, 2017), a preliminary selection of 29 station records from the KiK-net was made (Fig.1), and comparison plots of the simulated acceleration time series and the actual station-recorded acceleration time series were generated (Fig. 2). To simplify the computational workload in our subsequent research and to demonstrate the efficiency of the hybrid slip model in estimating ground motion, we further selected 10 stations for the hybrid slip model study based on the residual threshold between the simulated strong motion records generated by each station's Automatic Inversion Codes and the original records, from the aforementioned 29 stations. However, we found that the 10 stations selected by this procedure were all more than 50 km away from the source. To better study the strong motion characteristics in the near-field region, we manually added 3 near-field stations (with a source distance of <50 km), aiming to better reflect the near-field strong motion characteristics of this seismic event through this approach. As a result, a total of 13 high-quality station records were obtained. The locations of the reference stations and the epicenter are shown in Fig. 1.

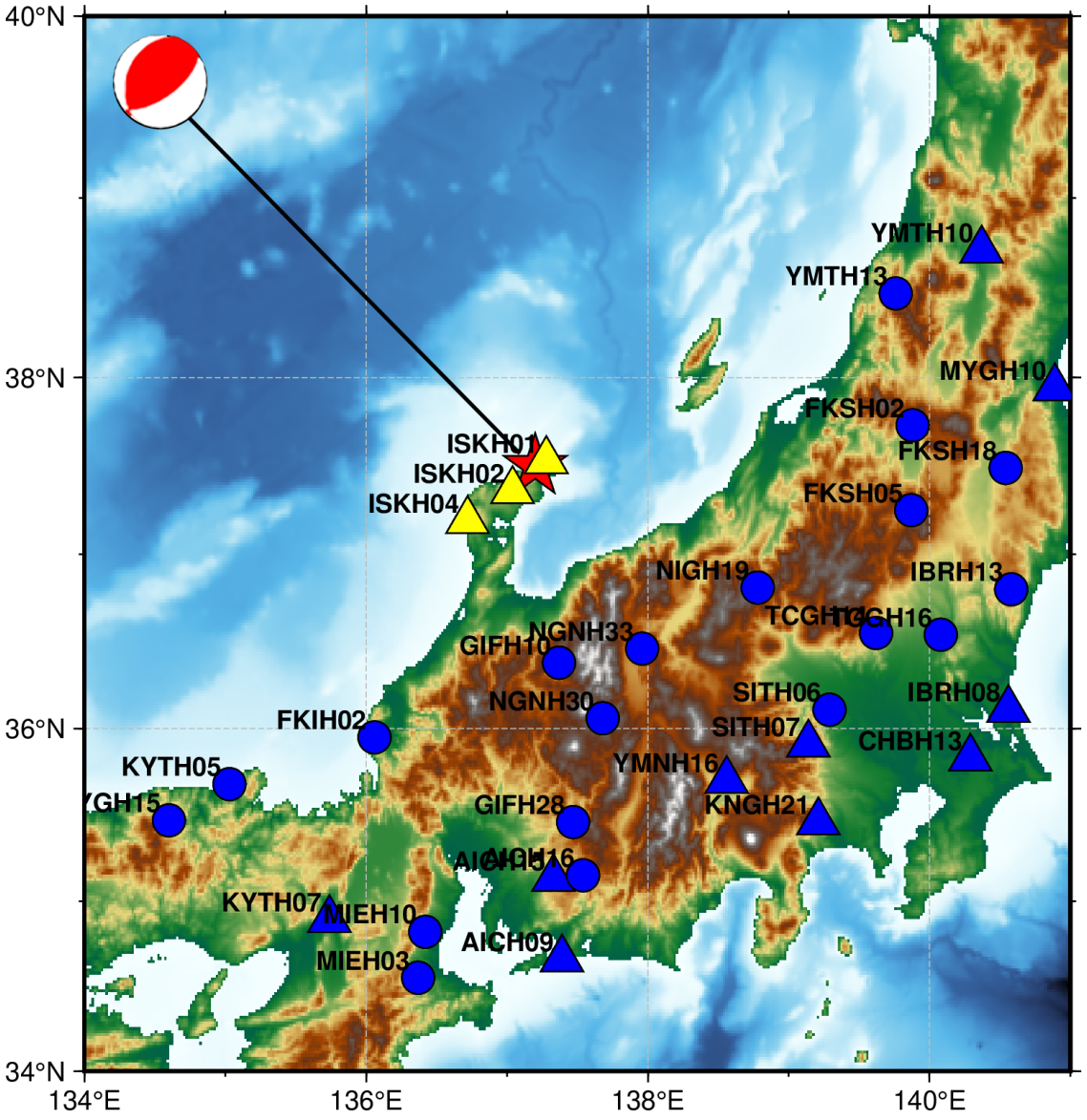

Figure 1. The epicenter location and the seismic stations of KiK-net. The red star indicates the location of the epicenter. The blue shapes represent the locations of the 29 stations selected by the Automatic Inversion Code. Among them, the blue triangles indicate the 10 stations that were selected for further study after applying the waveform fitting residual threshold. The yellow triangles represent the 3 manually added near-field stations (with a source distance of <50 km). The focal mechanism solution is sourced from the China Earthquake Networks Center. The base map data is sourced from the GMT global terrain relief dataset, IGPP Earth Relief.

3.2 Strong Motion Inversion

Based on the strong motion data recorded by the initial 29 stations and processed using the Automatic Inversion Codes, the unscaled static source rupture process corresponding to this seismic event was obtained (Fig. 3). To make the slip distribution appear more continuous and smooth, the Automatic Inversion Codes apply certain smoothing techniques to the slip values and adjust the inversion results according to the actual size of the fault. Figure 4 shows the locations of the 29 stations used in the inversion by the Automatic Inversion Codes, as well as the fault slip distribution after adjusting for size and smoothing. According to the inversion results, the fault scale of the Noto Peninsula earthquake is approximately 200 kilometers in length, with a depth along the dip of about 15 kilometers, providing a reference for establishing the global parameters needed for subsequent mixed sliding model. Figure 5 shows the source time functions on each subfault, indicating that seismic energy diffuses bidirectionally near the source, which can serve as a mechanism reference for subsequent finite fault modeling.

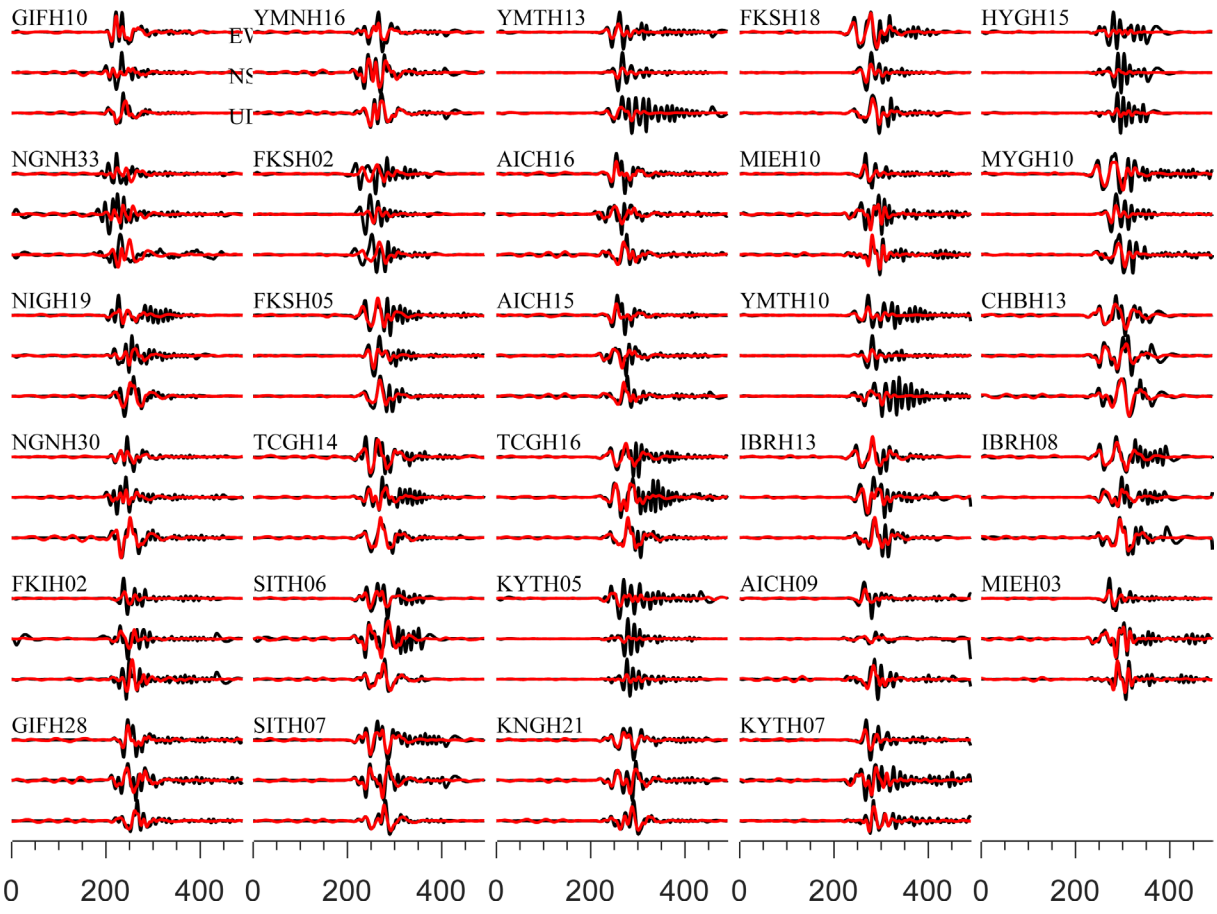

Figure 2. The simulated acceleration records of 29 stations were selected and compared with the actual records. Each station has three components: east-west, north-south, and vertical. The red line represents the inversion simulation record, and the black line represents the real station record.

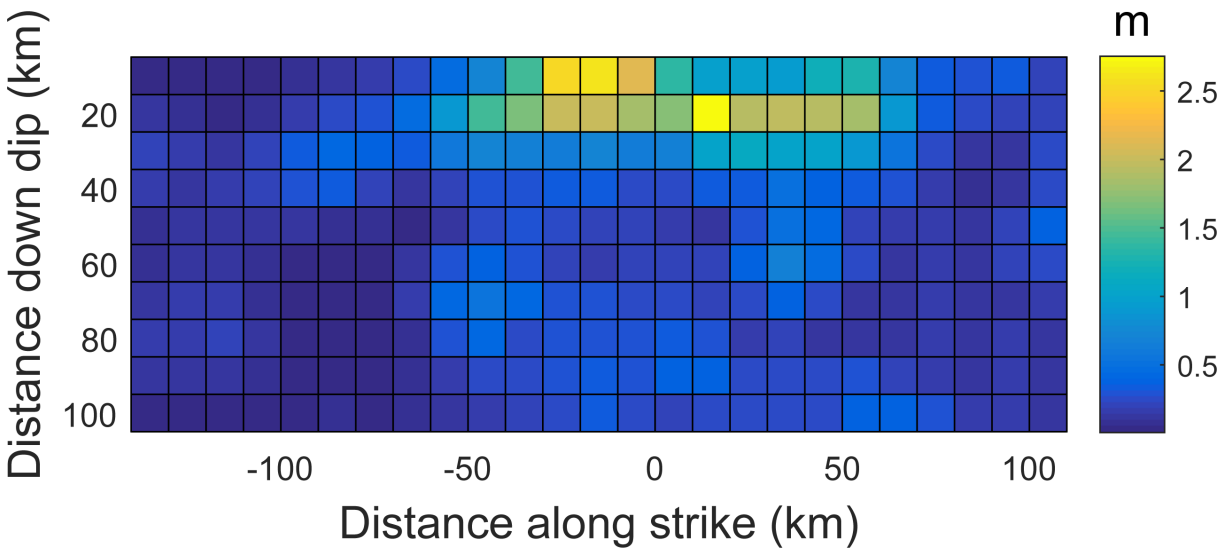

Figure 3. The original static source rupture process generated by the Automatic Inversion Code through strong motion inversion. The initial slip distribution, obtained from the inversion of strong motion data from the 29 stations preliminarily selected by the Automatic Inversion Code program. It is unadjusted for scale and without slip value smoothing. The program internally uses a fixed empirical relationship based on the moment magnitude to generate a fixed source parameter configuration.

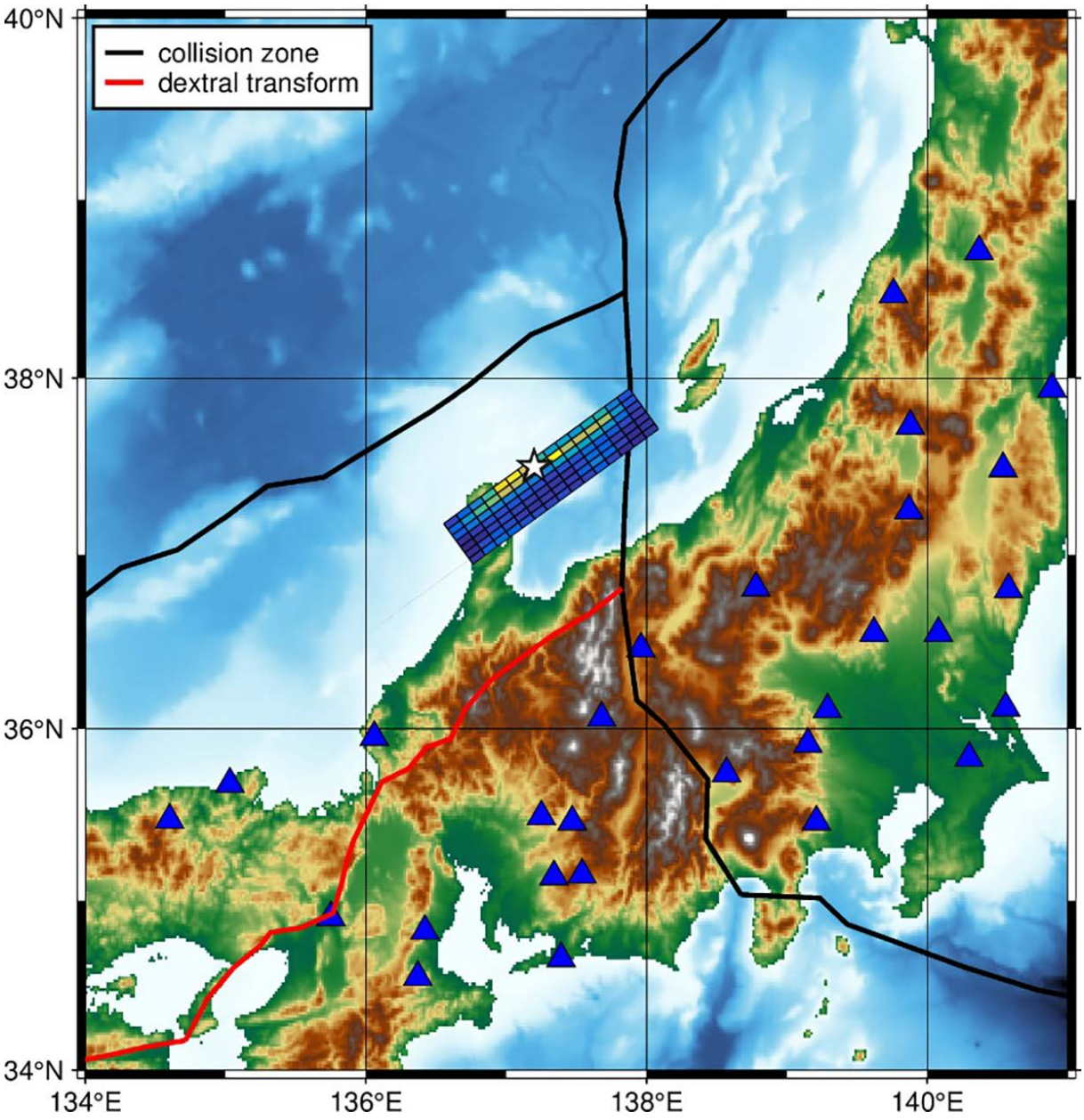

Figure 4. The adjusted source slip model and the location map of the initially selected 29 stations. The white star indicates the location of the epicenter, and the blue triangles represent the locations of the 29 stations initially selected by the inversion program. The different polylines represent the fault boundaries and their types. The slip distribution is the result of applying slip value smoothing and scale adjustment to the data in Fig. 3 using the Automatic Inversion Code, with the maximum slip value and the source rupture pattern remaining consistent with those in Fig. 3. The base map data is sourced from the GMT global terrain relief dataset and IGPP Earth Relief. Plate boundary data are derived from the Global Tectonic dataset in GMT.

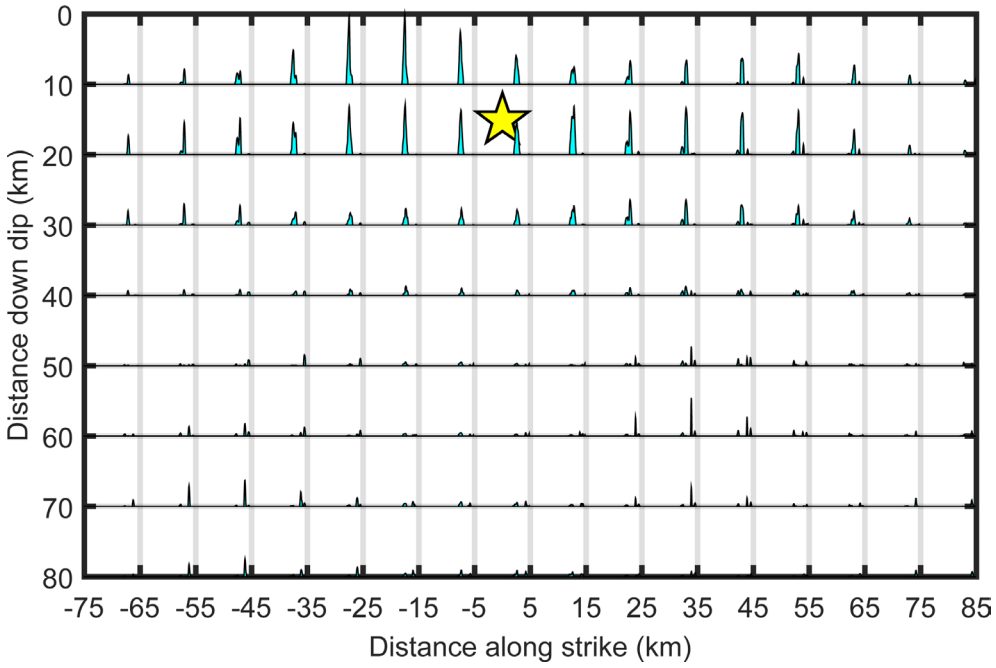

Figure 5. The sub-fault source time functions obtained through inversion of strong motion data from 29 stations using the Automatic Inversion Code. The yellow star indicates the fault source location, and the corresponding time functions are shown for each sub-fault.

4. The Application of Stochastic Finite Fault Method

4.1 Establishment of Finite Fault Source Models

Global Source Parameters

According to the moment tensor solution from the China Earthquake Networks Center, the focal mechanism of the mainshock is primarily characterized by reverse faulting with a component of left-lateral strike-slip (Fig. 1). Based on the actual geological background and the conclusions of Chen Guangqi (2024), a fault plane model with a strike of 52° dip of 62° is adopted, with a moment magnitude Mw = 7.6.

Based on the nature of the fault as a reverse fault, with $7.0 < M_w \leq 7.7$, a semi-empirical relationship formula for the macroscopic source parameters was adopted (Wang, 2004; Dang, 2022).

$$\text{Fault rupture area: } \log S = M_w - 4.20, \tag{6}$$

$$\text{Length of fault rupture: } \log L = 0.5M_w - 1.60, \tag{7}$$

$$\text{Width of fault rupture: } W = S/L, \tag{8}$$

$$\text{Average slip: } \log \overline{D} = 0.5M_w - 0.65, \tag{9}$$

The macroscopic source parameters (global source parameters) of the Mw7.6 earthquake were determined, and the rupture length and width were rounded to integers:

$$S = 3162 \text{ km}^2, \quad L = 178 \text{ km}$$
$$W = 18 \text{ km}, \quad \overline{D} = 1584.9 \text{ cm}$$

Local Source Parameters

The sliding distribution of the fault rupture during this earthquake was characterized using the hybrid sliding model method, identifying the positions of the largest and other asperities. The position of the largest asperity remained essentially unchanged, while the positions of the other asperities exhibited some randomness after applying certain constraints (using the fault plane as a boundary condition to ensure that the other asperities remained within the fault plane and did not significantly overlap with the largest asperity). The specific parameters of the sliding distribution model used in this study are shown in Table 1.

Types of local source parameters	Sliding distribution parameters	Parameters values
Asperities numbers	—	2
Area of asperities/km^2	Area of all asperities	602.56
	Area of the maximum asperity	416.87
	Area of the remaining asperity	185.69
Average slip on the asperity and fault plane /cm	Average on the maximum asperity	1258.9
	Average on the remaining asperity	1230.3
	Average on the fault plane	297.5
Center Location of the largest asperity/km	Along the fault length	93.33
	Along the fault width	6.03
Spatial corner wavenumber /km^{-1}	Along the fault length	0.0120
	Along the fault width	0.0275
Location of initiation point /km	Along strike	100
	Along dip	6.03

Table 1. Sliding distribution parameter table of the predicted January 1, 2024 Noto Peninsula earthquake (Mw7.6) in Japan.

The method and steps described above were used to generate 30 models of the slip distribution for the designated earthquake. Among these, the most effective source model was selected (Fig. 6). From Fig. 6, it can be observed that the determined parameters of the asperities stably represent the overall distribution characteristics of the slip. Meanwhile, the k^2 slip model exhibits significant random variations in the high-wave-number region. The model indicates that: the fault has an overall length of approximately 170 km along the strike direction and a width of about 18 km along the dip direction; The largest asperity is mainly located in the middle of the fault plane, with a total length of 90 km and a width of 10 km. The maximum slip value is approximately 4.0 meters, which is comparable to the maximum slip value provided by the USGS model (Fig. 7).

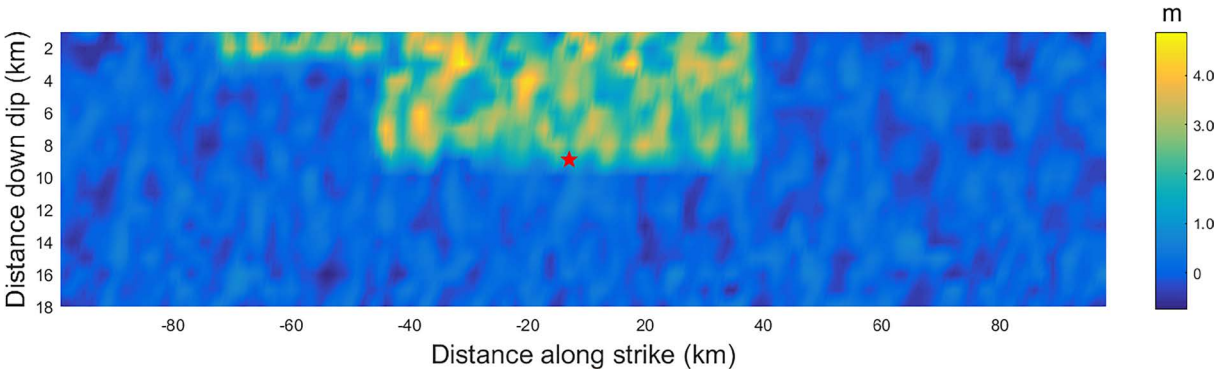

Figure 6. Hybrid Source model (HSM) estimated using semiempirical relationships of global and local source parameters. The red star represents the position of the fracture starting point of each slip model.

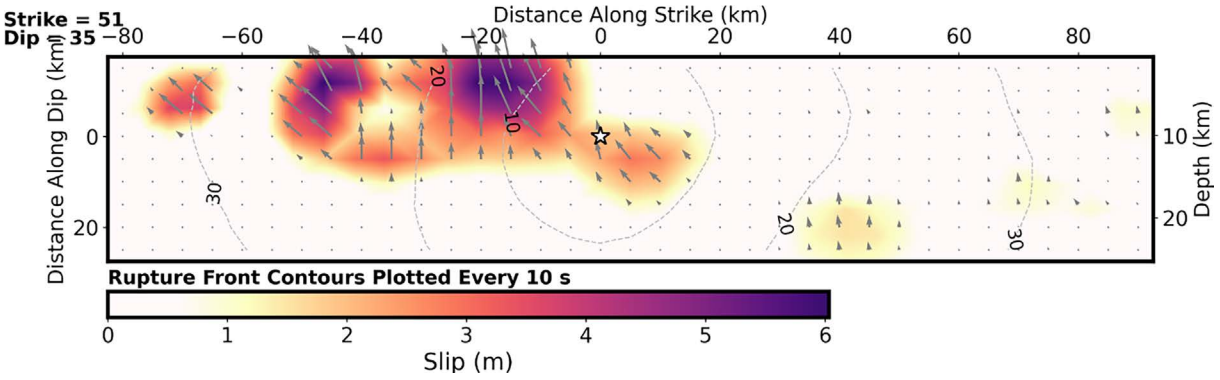

Figure 7. The cross-sectional view of the slip distribution based on GNSS data inversion from USGS. The strike direction is indicated above each fault plane and the hypocenter location is denoted by a star. Slip amplitude is shown in color and the motion direction of the hanging wall relative to the footwall (rake angle) is indicated with arrows. Contours show the rupture initiation time in seconds.

4.2 Stochastic Seismic Motion Synthesis Method

In the stochastic method, the path propagation function mainly involves determining geometric attenuation and quality factor. This paper adopts the geometric attenuation model proposed by Atkinson and Boore (1998) for the crustal layers above the Moho at a depth of 50 km:

$$Z(R)\begin{cases}\dfrac{1}{R}, & R < 70\ \text{km} \\ \dfrac{1}{70}, & 70\ \text{km} \le R < 130\ \text{km} \\ \dfrac{1}{70}\sqrt{\dfrac{130}{R}}, & 130\ \text{km} \le R\end{cases} \tag{10}$$

For the study area, the relationship between seismic quality factor and frequency in the Noto Peninsula seismic zone was referenced from Ghofrani (2013) and Zhou et al. (2021), and expressed as:

$$Q(f) = 58.02 f^{1.9508} \tag{11}$$

The duration of the path was determined using the empirical relationship proposed by Atkinson and Boore (1998) for the eastern region of North America.

$$\begin{cases} 0, & R < 10 \text{ km} \\ 0.16(R-1), & 10 \text{ km} \le R < 70 \text{ km} \\ 9.6 - 0.03(R-70), & 70 \text{ km} \le R < 130 \text{ km} \\ 7.8 + 0.04(R-130), & 130 \text{ km} \le R \end{cases} \tag{12}$$

Unlike classic method that uses a uniform function to calculate ground motions for all stations, this study divides the selected station locations into three regions (Fig. 4). Depending on the region each station is located in, certain parameter adjustments are made for each station based on Eq. (11), aiming to reflect the authenticity and rationality of the simulation. In summary, the parameters required for predicting near-fault ground motion at bedrock sites for the 2024 Noto Peninsula earthquake in Japan are summarized in Table 2.

To validate the applicability of the model used in this study and to more intuitively demonstrate the waveform fitting effect between the simulated strong ground motions and the actual station records, we calculated the simulated pseudo-acceleration response spectra (PSA) for all 29 stations, as well as the pseudo-acceleration response spectra(PSA) for the original records of each of the 29 stations. We divided the data into short-period (<1.5s), medium-period (1.5 s–3.0 s), and long-period (>3.0 s) ranges and calculated the relative error between the simulated and actual PSA for each station at different periods. Subsequently, we computed the mean and standard deviation of the relative errors for the 29 stations at different periods (Fig. 8). It was observed that, for most stations, the relative error values in the short-period range (1 s and 1.5 s) are less than 1 and close to 0, indicating that the model used in this study has high accuracy in predicting near-field high-frequency ground motions. However, in the long-period range, the ground motion errors at some stations are relatively larger, and there are even outliers. The reasons for these discrepancies may be related to the depth settings in the model and the complex geological conditions at certain stations, which can affect the strong motion records during the propagation of seismic waves.

Figure 9 shows the simulated and recorded pseudo-acceleration response spectra (PSA) for the selected bedrock stations from Fig. 8. During the simulation, the PSA values for stations KNGH21 and KYTH07 showed significant differences from the recorded values. This discrepancy could be due to the substantial directional difference between the station locations and the model fault plane, as well as the complex geological environment, which affected the simulation accuracy. For the other selected stations, the results indicate a high similarity between the predicted and recorded response spectra in the 0.1-10Hz range, demonstrating good fitting accuracy. Additionally, to compare the effectiveness of the hybrid slip model with the slip model obtained from strong motion inversion (Fig. 3) and the model provided by the USGS (Fig. 7), three near-field stations were selected for strong motion simulations using these three models. The results showed that all three models provided good fitting results (Fig. 10).

Parameters	Values
Fault orientation	Strike 54° Dip 62°
Fault dimension along strike and dip(km)	200 × 14
Depth of fault upper boundary(km)	9.6
Moment magnitude (M_w)	7.6
Sub-fault size (km)	1 × 1
Stress drop (10^5 Pa)	120

Parameters	Values
Slip distribution	Generated by the Hybrid Slip Model (Fig. 6)
Geometric attenuation	Eq. (10)
Path duration	Eq. (12)
Quality factor	Eq. (11)
Crustal amplification model	Boore and Joyner (1997) Typical Rock Site Model
Window Function	Saragoni-Hart Window
κ	0.035
Shear wave velocity of the crust ($km \cdot s^{-1}$)	3.7
Rupture velocity ($km \cdot s^{-1}$)	0.8 × Shear wave velocity
Density (g/cm^3)	2.8
Damping ratio (%)	5

Table 2. Ground motion prediction input parameters of the Noto Peninsula earthquake in Japan in 2024 near the fault bedrock site.

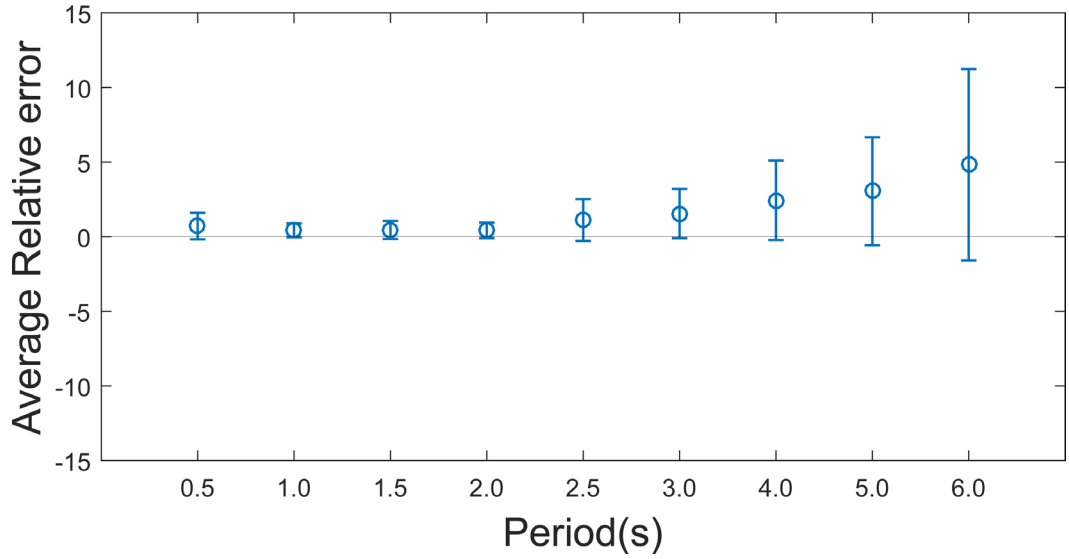

Figure 8. Mean and standard deviation of the relative error in fitting PSA between hybrid slip model simulations and strong motion records at different periods for 29 stations. The horizontal axis represents the selected periods; the dots represent the mean relative error of the 29 stations at different periods; the line segments indicate the variance of the relative error at different periods.

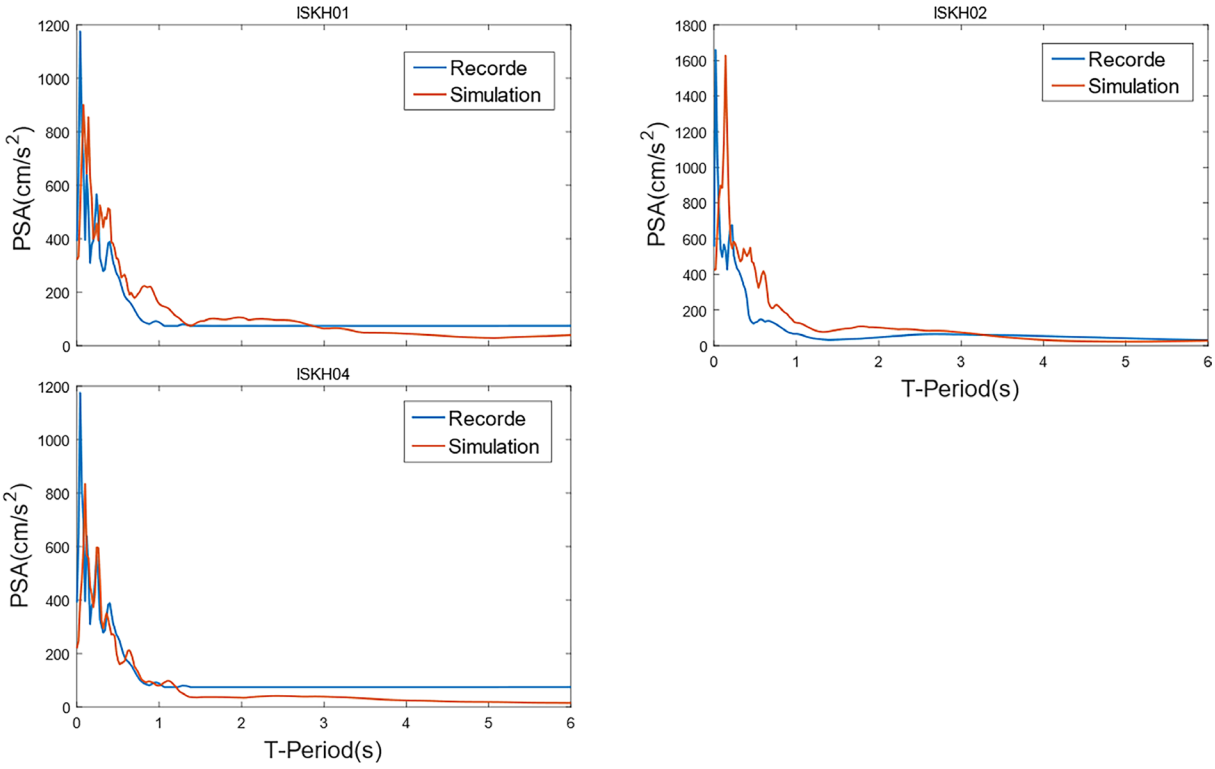

Figure 9. Comparison of acceleration response spectra simulated and recorded for the 2024 Noto Peninsula earthquake (Mw7.6) in Japan. The blue line represents the PSA from record strong motion, the red line represents the PSA obtained using the HSM.

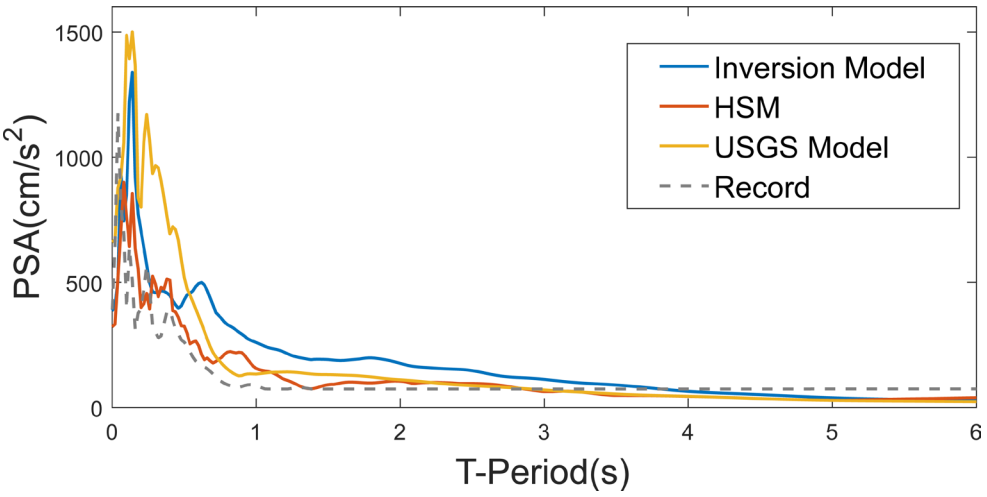

Figure 10. Comparison of ground motions from the HSM model and the strong motion inversion slip model at three stations. The blue line represents the PSA obtained using the inversion model, the red line represents the PSA obtained using the HSM, the yellow line represents the PSA obtained using USGS model, the grey line represents the record strong motion.

5. Conclusions

The finite fault source model established in this study utilizes the phase function of the k^2 slip model to represent the randomness of the source model, while employing asperities and global parameters to account for the determinism of the source model. Based on this hybrid slip model, the strong ground motion corresponding to this

earthquake event was simulated using the stochastic ground motion synthesis method (EXSIM). The results were compared with those from the strong motion inversion model, the source rupture model provided by the United States Geological Survey (USGS), and the actual records from the stations. The main conclusions are as follows:

1) Using the 2024 Noto Peninsula earthquake in Japan as an example, we initially screened 29 fundamental stations based on strong motion records from the KiK-net station network of the National Research Institute for Earth Science and Disaster Resilience (NIED) and the strong motion inversion method. Subsequently, 13 stations were manually selected for further finite fault method studies based on the fitting effectiveness of the strong motion time history records. Corresponding static source rupture processes and source time functions on sub-faults were generated. Under the geometric constraints of the inversion initial model, a finite fault hybrid source model was established. Combined with the source time functions, the results indicated that the fault rupture length was approximately 170 km, and the down-dip width was about 18 km. The rupture nucleated at the epicenter and extended bilaterally. The overall rupture duration was about 40 seconds, with a maximum co-seismic slip of approximately 5.0 meters on the fault plane, comparable to the 6.0 meters of the USGS slip model (Fig. 7). Comparing with the USGS source slip model (Fig. 7), we found that the geometric dimensions of the fault plane and the asperity locations on the ruptured fault are also very consistent with our results. Our model, based on the original numerical modeling, uses strong motion data as a constraint, making the model results not only closer to the real situation but also more reflective of the instantaneous effects during the earthquake. The USGS model, on the other hand, is derived from GNSS observations, teleseismic waveform data, and tsunami waveform records. These data characteristics focus more on long-period effects after the earthquake, and compared to our model, it can be seen that the USGS model still shows higher slip values in areas farther from the epicenter.
2) In the subsequent strong ground motion simulation, to avoid distortion in the simulation results for some stations due to differing geological conditions when using a uniform attenuation model, we built on the method for calculating the quality factor for Japan Eq. (11) proposed by Zhou et al. (2021). According to Fig. 4, we classified the previously selected 13 stations based on their tectonic regions and calculated the quality factor separately. Figure 8 shows the comparison between the simulated pseudo-acceleration response spectra (PSA) for some stations and the actual strong motion records. The results indicated that, after separately calculating the quality factor, the stations showed good fitting performance in both the short-period (1 second, 1.5 seconds) and long-period (3 seconds) ranges.
3) Using the above method, the PSA of the 29 selected stations were simulated and compared with the PSA of actual records to calculate the average relative error and standard deviation (Fig. 9). It was found that the fitting performance of the stations was good around the short-period, while there was a slight overestimation in the long-period range. This discrepancy may be related to the source depth set in the model and the site effects at each station. The results demonstrate that the hybrid slip model can efficiently and accurately predict strong ground motion without relying on extensive station data.
4) Similarly, we used the aforementioned finite fault method to compare the pseudo-acceleration response spectra of the Hybrid Slip Model (HSM) with those of the inversion slip model and the USGS model. We found that the overall fitting results of the HSM with these two models were quite good. In the short-period range (<1.5 seconds), compared to the model provided by the USGS, the simulated values of the HSM were closer to the actual station records, showing better fitting accuracy. In the long-period range (>3 seconds), the pseudo-acceleration response spectra values of the various models were comparable to the actual records.

Overall, the results presented in this paper are consistent with the slip models estimated from strong motion records and GNSS data, confirming the reliability and accuracy of the hybrid slip model. The stochastic method based on this model and dynamic corner frequency effectively simulates short-period high-frequency ground motion near the fault with a damping ratio of 5%. This indicates that the methods and procedures proposed in this paper for constructing finite fault source models on active faults and predicting strong ground motions are feasible and practical

Chen Guangqi et al. (2024) and the USGS both used the GNSS observation method, which requires consideration of constraints such as satellite clock errors, receiver clock errors, troposphere models, ionosphere models, and solid tide corrections during the inversion process. In contrast, the method used in this paper employs strong motion data from near-field stations to quickly and efficiently simulate the source rupture process and predict strong ground motion in the study area. The results of this study also provide a method for investigating the source rupture process, asperity distribution, and regional strong ground motion prediction for the Noto Peninsula earthquake.

Data availability statement. The code used to simulate seismic ground motion with the stochastic finite fault model can be obtained from the Engineering Seismology Toolbox (seismotoolbox.ca). The strong motion waveform data for the Noto Peninsula earthquake used in this study were provided by the National Research Institute for Earth Science and Disaster Resilience (NIED) in Japan. The Automatic Inversion Codes can be accessed from the Geophysical Source Academic Information Sharing group (pku-geophysics-source.group). The source rupture model published by USGS can be found at the following URL: M 7.5 – 2024 Noto Peninsula, Japan Earthquake (usgs.gov).

Acknowledgements. This research was supported by the Natural National Science Foundation for Young Scientists of China (Grant number 41704059). We thank the National Research Institute for Earth Science and Disaster Resilience (NIED) in Japan for providing the strong motion data. We are also thankful to Associate X. D. Sun of Southwest Jiaotong University for his guidance on the programming of the hybrid slip model used in this study.

References

Aki, K. (1967). Scaling Law of Seismic Spectrum, J. Geophys. Res. Atmos., 72, 4, 1217-1231, doi:10.1029/JZ072i004p01217.

Atkinson, G. M. and D. M. Boore (1998). Evaluation of models for earthquake source spectra in eastern North America, Bull. Seismol. Soc. Am., 88, 4, 917-934, doi:10.1785/bssa0880040917.

Beresnev, I. A. and G. M. Atkinson (1997). Modeling finite-fault radiation from the ωn spectrum, Bull. Seismol. Soc. Am., 87, 1, 67-84, doi:10.1785/BSSA0870010067.

Beresnev, I. A. and G. M. Atkinson (1998). FINSIM – a FORTRAN Program for Simulating Stochastic Acceleration Time Histories from Finite Faults, Seismol. Res. Lett, 69, 1, 27-32, doi:10.1785/gssrl.69.1.27.

Boore, D. M. (1983). Stochastic simulation of high-frequency ground motions based on seismological models of the radiated spectra, Bull. Seismol. Soc. Am., 73, 6A, 1865-1894.

Boore, D. M. (2003). Simulation of Ground Motion Using the Stochastic Method, Pure Appl. Geophys., 160, 3, 635-676, doi:10.1007/PL00012553.

Boore, D. M. (2009). Comparing Stochastic Point-Source and Finite-Source Ground-Motion Simulations: SMSIM and EXSIM, B. Seismol. Soc. Am., 99, 6, 3202-3216, doi:10.1785/0120090056.

Brune, J. N. (1970). Tectonic stress and the spectra of seismic shear waves from earthquakes, J. Geophys. Res., 75, 26, 4997-5009, doi:10.1029/JB075i026p04997.

Cesca, S., Y. Zhang, V. Mouslopoulou, R. Wang et al. (2017). Complex rupture process of the Mw7.8, 2016, Kaikoura earthquake, New Zealand, and its aftershock sequence, Earth Planet. Sci. Lett., 478, 110-120, doi:10.1016/j.epsl.2017.08.024.

Chen, G., Y. Wu, M. Xia et al. (2024). The M7.6 Earthquake in the Noto Peninsula, Japan, on January 1, 2024: Source Characteristics, Damage Overview, and Emergency Response, Earthquake, 44, 01, 141-152, doi:10.12196/j.issn.1000-3274.2024.01.010.

Dang, P. and Q. Liu (2020). Stochastic finite-fault ground motion simulation for the Mw6.7 earthquake in Lushan, China, Nat. Hazards, 100, 3, 1215-1241, doi:10.1007/s11069-020-03859-3.

Dang, P., Q. Liu, L. Ji and C. Wang (2020). Simulation of finite fault hybrid source models for the Mw6.6 Jiuzhaigou, China, earthquake, J. Seismol., 24, 6, 1255-1265, doi:10.1007/s10950-020-09968-7.

Dang, P., J. Cui, Y. Li and Q. Liu (2023). Estimation of a hybrid slip model and its application to stochastic simulation of the Mw6.6 earthquake on September 5, 2022, in Luding, China, Stoch. Env. Res. Risk A., 37, 4175-4196, doi:10.1007/s00477-023-02500-6.

Gallovič, F. (2002). High frequency strong motion synthesis for k-2 rupture models, PhD Dissertation, Charles University in Prague, https://geo.mff.cuni.cz/~gallovic/abst/Gallovic.Master.pdf.

Ghasemi, H., Y. Fukushima, K. Koketsu, H. Miyake et al. (2010). Ground-Motion Simulation for the 2008 Wenchuan, China, Earthquake Using the Stochastic Finite-Fault Method, Bull. Seismol. Soc. Am., 100, 5B, 2476-2490, doi:10.1785/0120090258.

Ghofrani, H., G. M. Atkinson, K. Goda and K. Assatourians (2013). Stochastic Finite-Fault Simulations of the 2011 Tohoku, Japan, Earthquake, Bull. Seismol. Soc. Am., 103, 2B, 1307-1320, doi:10.1785/0120120228.

Hamling, I. J., S. Hreinsdóttir, K. Clark, J. Elliott et al. (2017). Complex multifault rupture during the 2016 Mw7.8 Kaikōura earthquake, New Zealand, Science, 356, TN6334, 154, doi:10.1126/science.aam7194.

Hartzell, S. H. (1978). Earthquake aftershocks as Green's functions, Geophysics, 5, 1, 1-4, doi:10.1029/GL005i001p00001.

Hartzell, S. H. and J. N. Brune (1979). The horse canyon earthquake of August 2, 1975 – Two-stage stress-release process in a strike-slip earthquake, Bull. Seismol. Soc. Am., 69, 4, 1161-1173, doi:10.1785/BSSA0690041161.

Irikura, K. (2000). Prediction of Strong Ground Motions from Future Earthquakes Caused by Active Faults-Case of The Osaka Basin, Proceedings of the 12th World Conference on Earthquake Engineering, New Zealand National Society for Earthquake Engineering, Wellington, New Zealand, 1-10, ISBN:0958215448.

Motazedian, D. and G. M. Atkinson (2005). Stochastic Finite-Fault Modeling Based on a Dynamic Corner Frequency, Bull. Seismol. Soc. Am., 95, 3, 995-1010, doi:10.1785/0120030207.

Papageorgiou, A. S. and K. Aki (1983). A specific barrier model for the quantitative description of inhomogeneous faulting and the prediction of strong ground motion. Part II. Applications of the model, Bull. Seismol. Soc. Am., 73, 4, 953-978, doi:10.1063/1.448683.

Song, J., P. Dang and J. Cui (2023). Composite Source Model for Broadband Ground-Motion Simulations: 2021 Mw7.4 Maduo, China, Earthquake Case Study, Seismol. Res. Lett., 94, 6, 2609-2626, doi:10.1785/0220230035.

Sun, X. D. (2010). Research on Several Issues in Estimation of Strong Ground Motion Fields, PhD Dissertation, Harbin Institute of Technology, Harbin.

Tao, X., H. Liu, D. Zhang et al. (2009). Establishment of Source Models in Near-Field Ground Motion Prediction, in proceedings of the Fourth National Symposium on Earthquake Resistance and Disaster Reduction Engineering: New Advances in Theory and Practice of Seismic Disaster Reduction, Commemorating the First Anniversary of the Wenchuan Earthquake, China Civil Engineering Society, Chinese Academy of Engineering, Department of Civil, Hydraulic and Architectural Engineering, China Society for Earthquake Disaster Prevention and Mitigation Technology Promotion, Fujian Civil Engineering and Architecture Society (Editors), Beijing, 8, ISBN: 9787112109234.

Ugurhan, B. and A. Askan (2010). Stochastic Strong Ground Motion Simulation of the 12 November 1999 Düzce (Turkey) Earthquake Using a Dynamic Corner Frequency Approach, Bull. Seismol. Soc. Am., 100, 4, 1498-1512, doi:10.1785/0120090358.

Wang, H. (2004). Finite Fault Source Model for Predicting Near-Field Strong Ground Motion, PhD Dissertation, Institute of Engineering Mechanics, China Earthquake Administration.

Wang, R., S. Heimann, Y. Zhang, H. Wang et al. (2017). Complete synthetic seismograms based on a spherical self-gravitating Earth model with an atmosphere-ocean-mantle-core structure, Geophys. J. Int., 210, 3, 1739-1764, doi:10.1093/gji/ggx259.

Zafarani, H., M. Rahimi, A. Noorzad, B. Hassani et al. (2015). Stochastic Simulation of Strong-Motion Records from the 2012 Ahar-Varzaghan Dual Earthquakes, Northwest of Iran, Bull. Seismol. Soc. Am., 105, 3, 1419-1434, doi:10.1785/0120140241.

Zeng, Y., J. G. Anderson and G. Yu (1994). A composite source model for computing realistic synthetic strong ground motions, Geophys. Res. Lett., 21, 8, 725-728, doi:10.1029/94GL00367.

Zhang, Y., R. Wang, J. Zschau, Y. Chen et al. (2014). Automatic imaging of earthquake rupture processes by iterative deconvolution and stacking of high-rate GPS and strong motion seismograms, J. Geophys. Res. Solid Earth, 119, 7, 5633-5650, doi:10.1002/2013JB010469.

Zheng, X., Y. Zhang, R. Wang, L. Zhao et al. (2020). Automatic Inversions of Strong-Motion Records for Finite-Fault Models of Significant Earthquakes in and Around Japan, J. Geophys. Res. Solid Earth, 125, 9, e2020JB019992, doi:10.1029/2020JB019992.

***CORRESPONDING AUTHOR: Zhuofan YANG**,
School of Earth Sciences, Yunnan University, Yunnan, China
e-mail: yangzhuofan@stu.ynu.edu.cn